CHEMPHYSCHEM

Supporting Information

Triphilic Ionic-Liquid Mixtures: Fluorinated and Non-fluorinated Aprotic Ionic-Liquid Mixtures

Oldamur Hollóczki,[a] Marina Macchiagodena,[a] Henry Weber,[a] Martin Thomas,[a] Martin Brehm,[b] Annegret Stark,[c] Olga Russina,[d] Alessandro Triolo,[e] and Barbara Kirchner*[a]

cphc_201500473_sm_miscellaneous_information.pdf

Supporting information:

1 Color figures

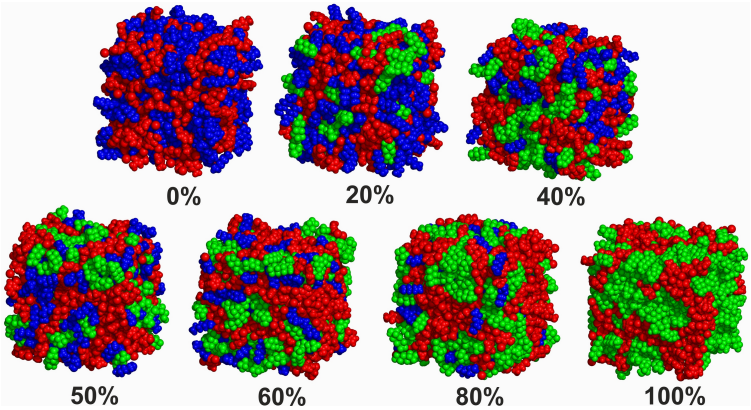

Figure 1: Colored snapshots of $[C_8C_1Im][Br]$ mixed with $[(C_F)_6C_2C_1Im][Br]$, simulated at 300 K. The percentage of the FAIL is indicated by the number below each system.

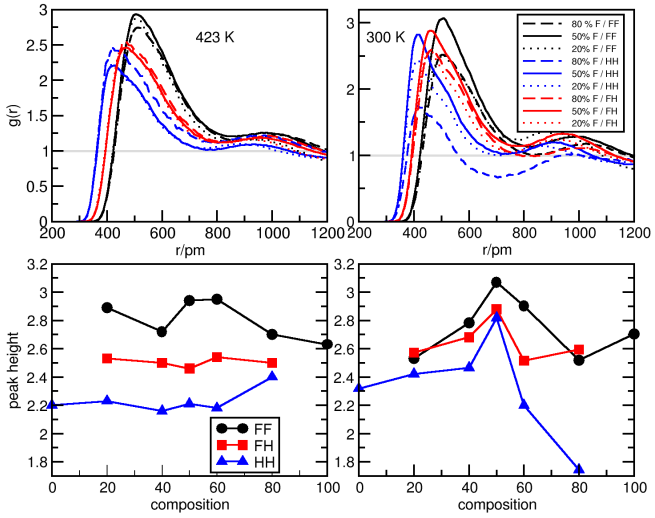

Figure 2: Selected radial distribution functions (left: 423 K, right: 300 K) of $[C_8C_1Im][Br]$ mixed with $[(C_F)_6C_2C_1Im][Br]$. FF indicates the C_{term}-C_{term} function from the fluorinated side chains, HH the C_{term}-C_{term} function from the alkyl side chains and FH, the C_{term}-C_{term} function where one carbon atom stems from the fluorinated side chain and the other one from the alkyl side chain. Below is shown the peak height plotted against the composition of the system.

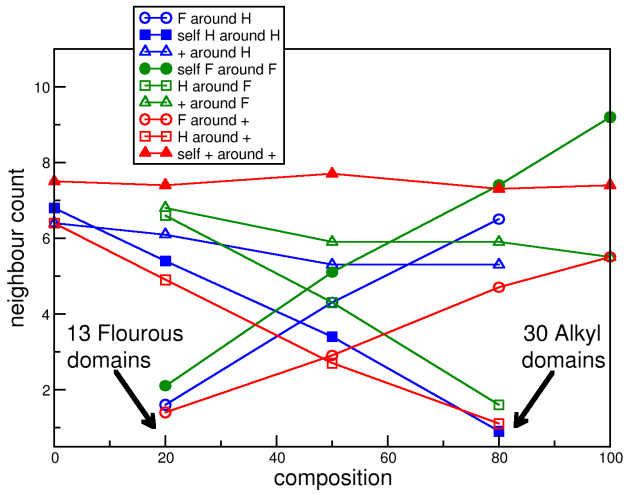

Figure 3: Neighbor count from table 4 plotted against the composition of $[C_8C_1Im][Br]$ mixed with $[(C_F)_6C_2C_1Im][Br]$. F: Fluorous; H: Alkyl and +: Ring moieties. Blue: neighbor count around Alkyl, green around Fluorous and red around polar Ring groups.

Table 1: Different simulation set ups and obtained average densities ρ in g cm^{-3}.

system		size	T	ρ	
FAIL	IL		[K]	300 K	423 K
50%	50%	1024	423; 300	–	–
0%	100%	260	423; 300	1.11	1.02
20%	80%	260	423; 300	1.24	1.15
40%	60%	260	423; 300	1.36	1.26
50%	50%	260	423; 300	1.42	1.31
60%	40%	260	423; 300	1.47	1.36
80%	20%	260	423; 300	1.57	1.44
100%	0%	260	423; 300	1.65	1.53

2 Computational methodologies and systems investigated

Classical molecular dynamics (MD) was employed to study the two different cations $[(C_F)_6C_2C_1Im]^+$ (termed FAIL) and $[C_8C_1Im]^+$ (termed IL) in combination with the bromide anion at different particle numbers, temperatures and mole fractions resulting in 16 different simulations. Details are given in table 1.

The large systems with 1024 ion pairs (table 1) were simulated at the obtained densities of the corresponding 260 ion pair system, which led to box sizes of 7781.16 pm at 300 K and 7990.28 pm at 423 K. All details were taken as in the 260 ion pair simulations, see following paragraphs. The parameter which are not listed in this section were taken from Ref.[1]

The simulations were carried out using the LAMMPS program package[2] always employing periodic boundary conditions with a time step of 1 fs. In order to execute the molecular

dynamics simulations, an AMBER kind force field[3] of the form

$$
\begin{aligned}
E_{\text{pot}} = & \sum_{\text{bonds}} K_r (r - r_0)^2 \\
& + \sum_{\text{angles}} K_\theta (\theta - \theta_0)^2 \\
& + \sum_{\text{dihedrals}} K_\phi \left[1 + d \cos(n\phi)\right] \\
& + \sum_{\text{improper}} K_\chi (\chi - \chi_0)^2 \\
& + \sum_{i<j} \left\{ 4\, \varepsilon_{ij} \left[\left(\frac{\sigma_{ij}}{r_{ij}} \right)^{12} - \left(\frac{\sigma_{ij}}{r_{ij}} \right)^{6} \right] + \frac{C q_i q_j}{\epsilon r_{ij}} \right\} \quad ,
\end{aligned}
\tag{1}
$$

with the respective energy constants K for bonded interactions, namely bonds, angles, dihedrals and improper torsion angles was used. Non-bonded interactions were described by the 6-12 Lennard-Jones potential. Lorentz–Berthelot mixing rules[4,5] ($\varepsilon_{ij} = \sqrt{\varepsilon_i \varepsilon_j}$ and $\sigma_{ij} = (\sigma_i + \sigma_j)/2$) were applied to obtain unlike atom parameters. Interaction between 1-4 bonded atoms was scaled by 0.5 for the Lennard-Jones part and by 0.833 (=5/6) for Coulombic interactions. Lennard-Jones and Coulombic interactions were computed within the cutoff radius $r_c = 1.6$ nm, regarding $r_{ij} = |r_i - r_j| < r_c$. Coulombic interaction energies beyond the cutoff radius were computed via the particle-particle particle-mesh solver[6] with an accuracy of 10^{-5}, referred to the RMS force error in reciprocal space regarding Eq. 38 of Deserno.[7] Force field constants for imidazolium and fluoroalkylimidazolium ILs adopted to fit Eq. 1 were applied.[8–11]

Atomic charges q_i were derived from a restrained electrostatic potential (RESP) fit,[12] computed as follows:

1. The single isolated ion is geometry-optimized with density functional theory (DFT),[13,14] employing the B-LYP functional,[15,16] DZVP-MOLOPT basis set[17] and Goedecker–Teter–Hutter pseudopotentials[18,19] as well as dispersion correction D3 introduced by Grimme.[20,21]

2. The wave function of the geometry-optimized ion is derived in a pure Hartree–Fock calculation with the 6-31++G** basis set[22,23] and full atom potential.

3. The RESP fit is done with the obtained wave function and total charge of the system is set to $\pm 1e$.

4. Derived charges q_i are scaled with factor 0.8, see tables. 2 and 3.

Quantum chemical calculations were done employing the QUICKSTEP module[24] within the CP2K program package.

All simulations were carried out according to the following protocol:

1. The simulation cells were built up by replication of one, two or five ion pairs. The numbers were chosen to obtain the required mole fraction.

2. A short simulation to disorder the initial configuration was performed within the NVT-ensemble, with Nosé–Hoover-chain thermostats ($T = 600$ K, $\tau = 100$ fs).

3. An isobaric-isothermal simulation at 1 bar was performed within the NpT-ensemble for at least 1 ns. The temperature was $T = 300$ K or $T = 423$ K. The averaged cell vector of the last 500 ps was taken to perform the production run. Constant pressure and temperature was provided via Nosé–Hoover-chain thermostats at $T = 423$ K and the time constant of the thermostat ($\tau = 100$ fs) and the Nosé–Hoover barostat ($p = 1$ bar, $\tau = 1000$ fs).[25–27]

4. An equilibration of 1 ns preceded the production run, performed for 10 ns in the NVT-ensemble. The NVT-ensemble with Nosé–Hoover-chain thermostats at the different temperatures and the time constant of the thermostat $\tau = 100$ fs was employed.

The following colors were chosen for the snapshots of the simulation cells: polar, charge-bearing moieties of anions (bromide, -(SO2)2N-, and cations (imidazolium ring, C2H4 spacer and CH3) = red, unpolar alkyl = blue, fluoroalkyl = green.

Table 2: Partial atomic charges in atomic units of the coordinating atoms as employed in the simulation for the cation $[(C_F)_6C_2C_1Im]^+$.

atom	q [e]	atom	q [e]	atom	q [e]
C2	0.006510	H(Me)	0.125187		
N2	0.111898	C(1)	−0.109416	C(5)	0.139933
N3	0.047562	H(C1)	0.109254	F(C5)	−0.051883
C4	−0.106205	C(2)	−0.045113	C(6)	0.116663
C5	−0.228858	H(C2)	0.097386	F(C6)	−0.065865
H4	0.198189	C(3)	0.213363	C(7)	0.152102
H5	0.224275	F(C3)	−0.118670	F(C7)	−0.088636
H2	0.160641	C(4)	0.072057	C(term)	0.405328
C(Me)	−0.179225	F(C4)	−0.072382	F(term)	−0.124557

Table 3: Partial atomic charges in atomic units of the coordinating atoms as employed in the simulation $[(C_8C_1Im]^+$.

atom	q [e]	atom	q [e]	atom	q [e]
C2	−0.028258	H(Me)	0.106737		
N2	0.041974	C(1)	−0.068919	C(5)	0.010621
N3	0.111282	H(C1)	0.092110	H(C5)	−0.014132
C4	−0.166238	C(2)	0.014028	C(6)	0.039022
C5	−0.153210	H(C2)	−0.007818	H(C6)	−0.002289
H4	0.203744	C(3)	0.047682	C(7)	0.035902
H5	0.202349	H(C3)	−0.007818	H(C7)	0.001944
H2	0.203744	C(4)	−0.003086	C(term)	−0.127654
C(Me)	−0.148518	H(C4)	0.001750	H(term)	0.031922

3 Additional results

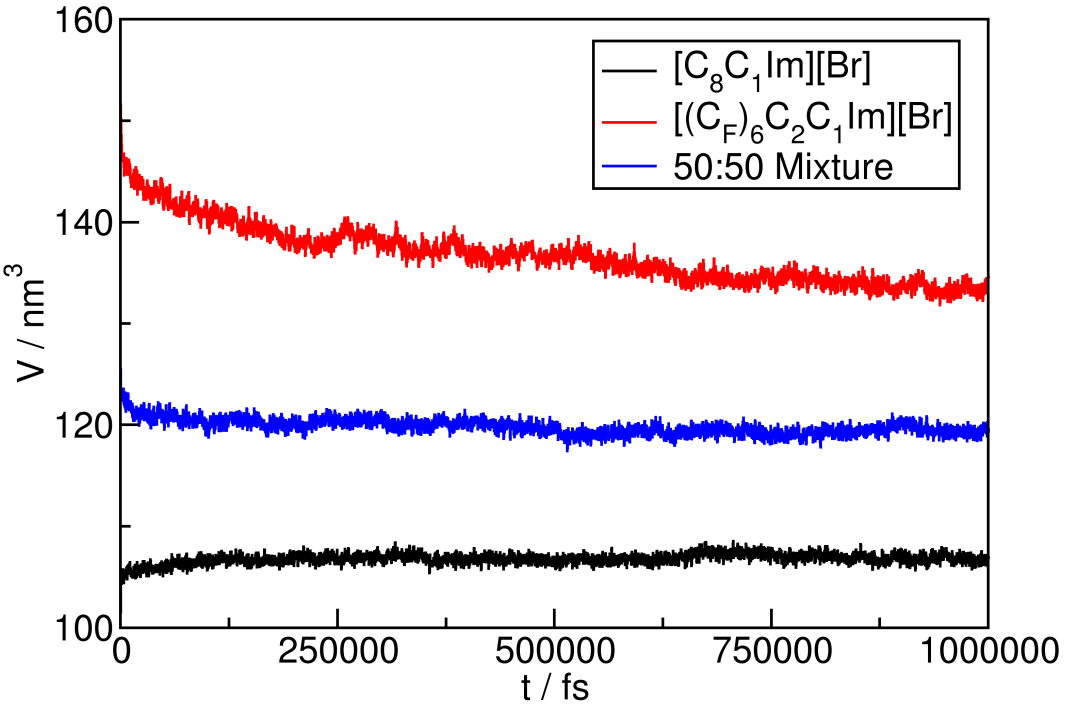

Figure 4: Cell volume plotted against the time in the NpT-ensemble simulations at ambient temperature.

In Fig. 4 we show the density changes within our first equilibium phase, namely the NpT-ensemble simulations. Shown is the cell volume during the simulation time. It is visible that the convergence of the system is slow for the FAIL system, but it converges within a ns.

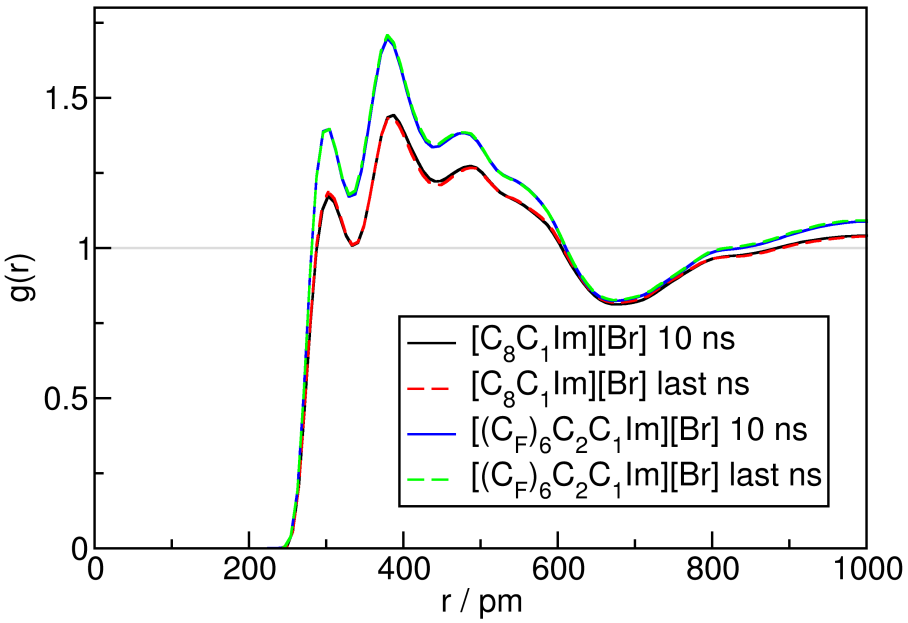

Figure 5: Radial distribution function.

Figure 5 shows the radial distribution function (RDF) in order to illustrate the behavior at the beginning and at the end of the production run. Shown is the anion-cation RDF, so the distance between all atoms of the cation to the anion, once for the complete trajectory and once for the last ns. It is obvious that there are no changes within the structure, therefore we deduce a sufficient convergence of also the structure which is necessary in order to discuss microheiterogeneity.

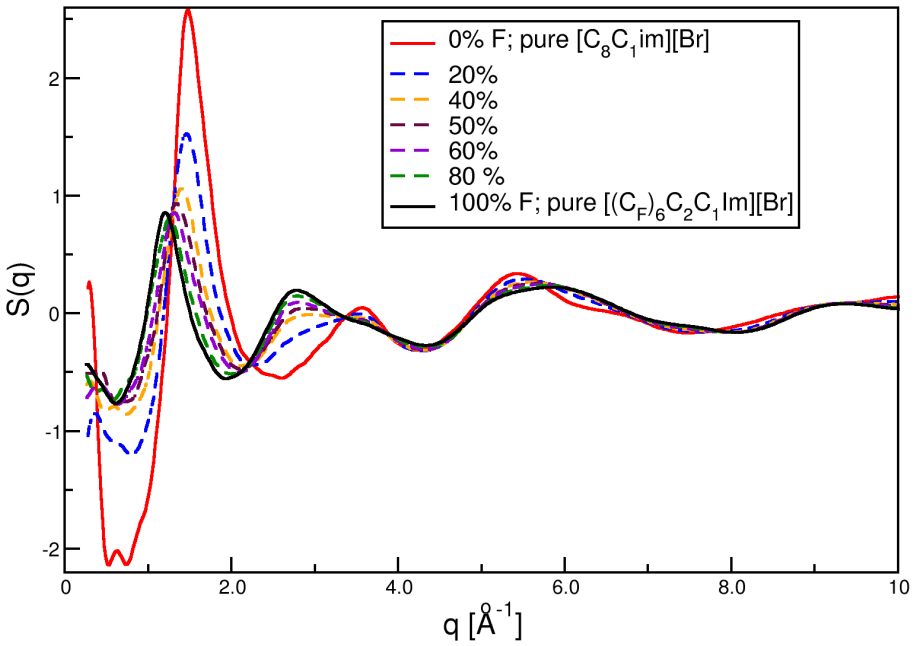

Figure 6: The $S(q)$ as calculated from eq. 3 of 260 ion pairs $[C_8C_1Im][Br]$ mixed with $[(C_F)_6C_2C_1Im][Br]$ in all calculated mole fractions at 423 K.

Comparing the different mole fractions it is apparent that upon introduction of the fluorous side chain system the peaks below 4 $Å^{-1}$ are shifted to lower q values while the peaks above are shifted to higher q values. Furthermore, the intensity decreases for the big peak at 1.5 $Å^{-1}$ but it increases at the peak of 3.6 $Å^{-1}$.

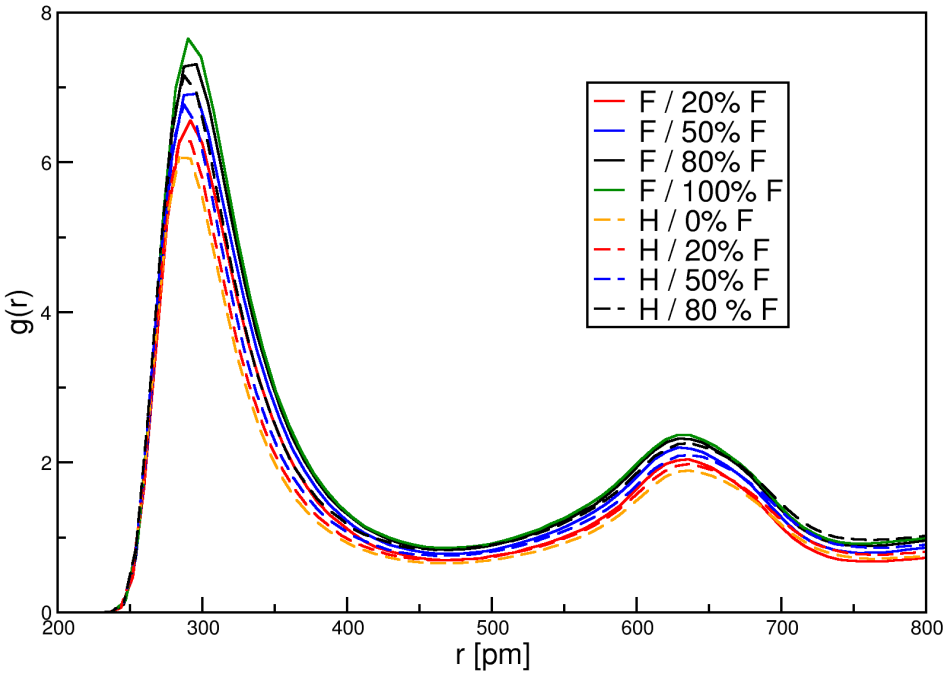

Figure 7: H2-Br RDFs of $[C_8C_1Im][Br]$ mixed with $[(C_F)_6C_2C_1Im][Br]$.

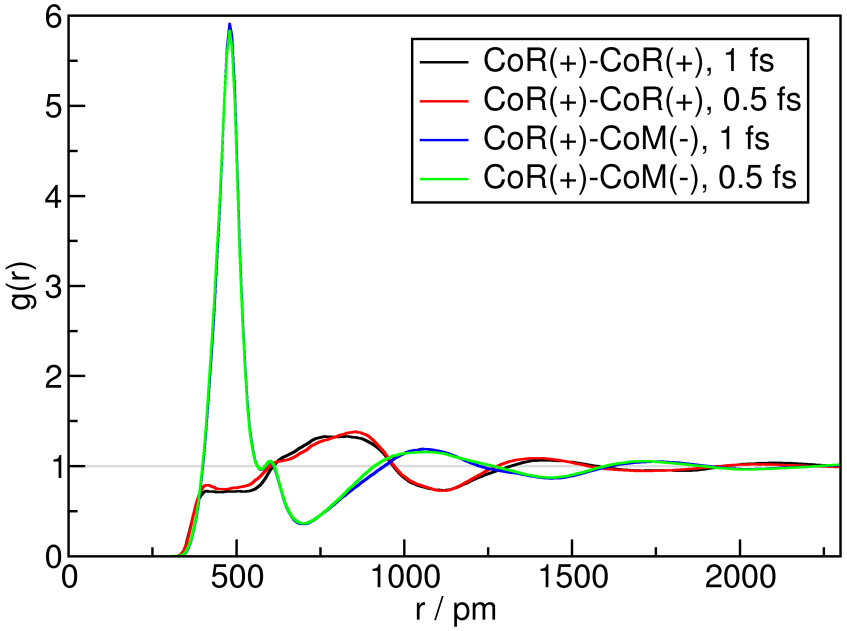

Figure 8: Center of mass RDFs of $[C_8C_1Im][Br]$ for different time steps at 300 K.

Table 4: Domain analysis. Column three to six list the neighbor count. Next to the domain count, the domain volume (D-Vol) and surface (D-Surf) together with average isoperimetric quotient (Q^{peri}) are given. Please note for the last three columns ring and anion are summarized as "polar group", therefore only data for the ring is given.

System			Fluorous	Alkyl	Ring	Anion	Domain-count	D-Vol Å^3	D-Surf Å^2	Q^{peri}
Fluorous	423 K	20:80	2.1	7.2	6.4	3.1	12.1	1337.0	1062.0	0.53
		50:50	5.3	4.3	5.8	2.8	1.5	31126.3	18047.4	0.23
		80:20	8.0	1.7	5.5	2.6	1.1	61448.4	24586.1	0.19
		FAIL	9.5	–	5.4	2.5	1.0	80513.7	23880.9	0.23
Alkyl	423 K	IL	–	7.3	6.3	3.1	1.1	49982.6	25401.0	0.16
		20:80	1.8	5.7	5.9	2.9	1.4	35702.3	22578.9	0.19
		50:50	4.3	3.4	5.5	2.6	5.2	6223.4	4981.9	0.47
		80:20	6.7	1.4	4.9	2.3	20.4	559.4	527.8	0.56
Ring	423 K	IL	–	6.3	7.5	5.0	1.0	63601.6	26871.8	0.15
		20:80	1.3	4.8	7.5	5.0	1.0	63246.5	25919.6	0.16
		50:50	2.9	2.7	7.7	5.1	1.0	63186.2	24418.0	0.18
		80:20	4.4	1.0	7.7	5.1	1.0	63107.5	23482.5	0.19
		FAIL	5.4	–	7.6	5.1	1.0	63006.1	23880.9	0.18
Anion	423 K	IL	–	3.1	5.0	0.2	–	–	–	–
		20:80	0.6	2.3	5.0	0.2	–	–	–	–
		50:50	1.4	1.3	5.1	0.3	–	–	–	–
		80:20	2.1	0.5	5.1	0.3	–	–	–	–
		FAIL	2.5	–	5.1	0.3	–	–	–	–

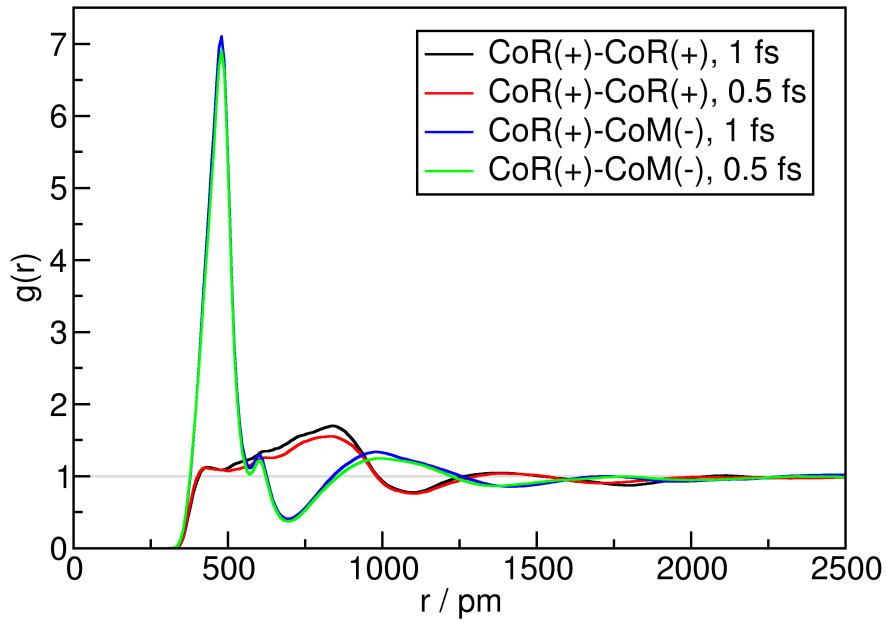

Figure 9: Center of mass RDFs of $[(C_F)_6C_2C_1Im][Br]$ for different time steps at 300 K.

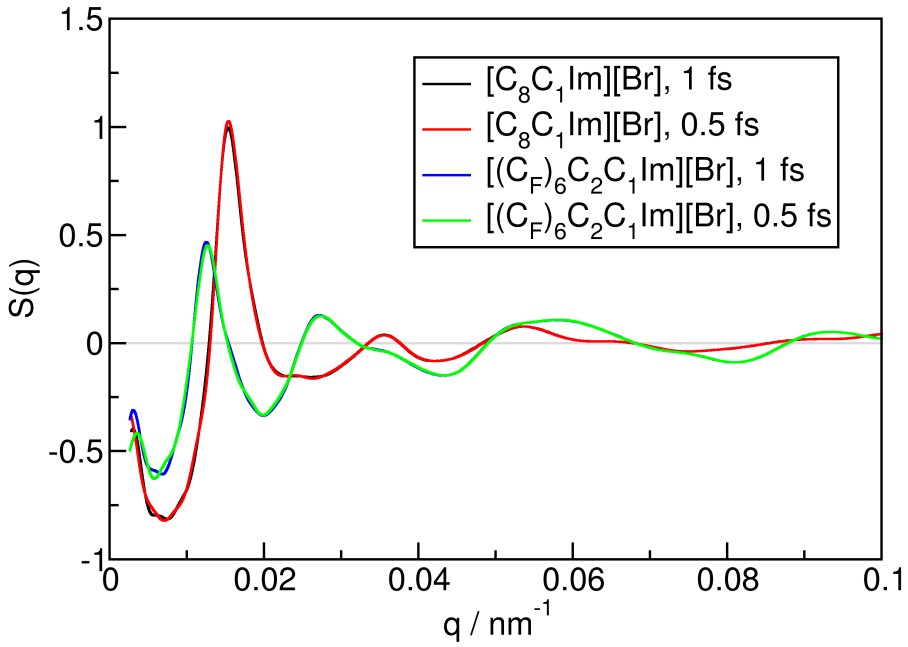

Figure 10: Structure factor of $[C_8C_1Im][Br]$ and of $[(C_F)_6C_2C_1Im][Br]$ with different time step.

References

[1] H. Weber, O. Hollóczki, A. S. Pensado, B. Kirchner, *J. Chem. Phys.* **2013**, *139*, 084502.

[2] S. Plimpton, *J. Comp. Phys.* **1995**, *117*, 1–19, http://lammps.sandia.gov.

[3] W. D. Cornell, P. Cieplak, C. I. Bayly, I. R. Gould, K. M. Merz, D. M. Ferguson, D. C. Spellmeyer, T. Fox, J. W. Caldwell, P. A. Kollman, *J. Am. Chem. Soc.* **1995**, *117*, 5179–5197.

[4] H. A. Lorentz, *Ann. Phys.* **1881**, *248*, 127–136.

[5] D. Berthelot, *Comptes rendus hebdomadaires des séances de l'Académie des Sciences* **1898**, *126*, 1703–1855.

[6] R. W. Hockney, J. W. Eastwood, *Computer Simulation Using Particles*, Adam Hilger, **1989**.

[7] M. Deserno, C. Holm, *J. Chem. Phys.* **1998**, *109*, 7694–7701.

[8] J. N. Canongia Lopes, J. Deschamps, A. Pádua, *J. Phys. Chem. B* **2004**, *108*, 2038–2047.

[9] J. N. Canongia Lopes, A. Pádua, *J. Phys. Chem. B* **2004**, *108*, 16893–16898.

[10] J. N. Canongia Lopes, A. Pádua, *J. Phys. Chem. B* **2006**, *110*, 19586–19592, PMID: 17004824.

[11] K. Shimizu, D. Almantariotis, M. F. Costa Gomes, A. A. H. Pádua, J. N. Canongia Lopes, *J. Phys. Chem. B* **2010**, *114*, 3592–3600.

[12] U. C. Singh, P. A. Kollman, *J. Comp. Chem.* **1984**, *5*, 129.

[13] P. Hohenberg, W. Kohn, *Phys. Rev. B* **1964**, *136*, B864–&.

[14] W. Kohn, L. Sham, *Phys. Rev.* **1965**, *140*, 1133–&.

[15] A. Becke, *Phys. Rev. A* **1988**, *38*, 3098–3100.

[16] C. Lee, W. Yang, R. Parr, *Phys. Rev. B* **1988**, *37*, 785–789.

[17] J. VandeVondele, J. Hutter, *J. Chem. Phys.* **2007**, *127*, 114105.

[18] S. Goedecker, M. Teter, J. Hutter, *Phys. Rev. B* **1996**, *54*, 1703–1710.

[19] C. Hartwigsen, S. Goedecker, J. Hutter, *Phys. Rev. B* **1998**, *58*, 3641–3662.

[20] S. Grimme, S. Ehrlich, L. Goerigk, *J. Comp. Chem.* **2011**, *32*, 1456–1465.

[21] S. Grimme, J. Antony, S. Ehrlich, H. Krieg, *J. Chem. Phys.*

[22] W. Hehre, R. Ditchfield, J. Pople, *J. Chem. Phys.* **1972**, *56*, 2257–&.

[23] M. Francl, W. Pietro, W. Hehre, J. Binkley, M. Gordon, D. Defrees, J. Pople, *J. Chem. Phys.* **1982**, *77*, 3654–3665.

[24] J. VandeVondele, M. Krack, F. Mohamed, M. Parrinello, T. Chassaing, J. Hutter, *Comput. Phys. Commun.* **2005**, *167*, 103–128.

[25] S. Nosé, *J. Chem. Phys.* **1984**, *81*, 511–519.

[26] S. Nosé, *Mol. Phys.* **1984**, *52*, 255–268.

[27] G. Martyna, M. Klein, M. Tuckerman, *J. Chem. Phys.* **1992**, *97*, 2635–2643.